Nanoscale Advances

ROYAL SOCIETY OF CHEMISTRY

PAPER

View Article Online
View Journal | View Issue

Cite this: *Nanoscale Adv.*, 2025, **7**, 7976

Preparation and characterization of nano guar gum/BF_3/Fe_3O_4 as a novel bio-based Lewis acid catalyst for the one-pot green synthesis of pyrimido benzothiazoles under solvent-free conditions

Motahare Hajihasani Bafghi,[a] Abdolhamid Bamoniri *[a] and Bi Bi Fatemeh Mirjalili [b]

Received 27th February 2025
Accepted 6th October 2025

DOI: 10.1039/d5na00201j

rsc.li/nanoscale-advances

Nano guar gum/BF_3/Fe_3O_4 is a bio-based nanocatalyst that was prepared, characterized and applied in one-pot three-component reactions of various aldehydes, 2-aminobenzothiazole and ethyl acetoacetate for the synthesis of 4*H*-pyrimido[2,1-*b*]benzothiazole derivatives at 80 °C under solvent-free conditions. The structure and properties of the heterogeneous bifunctional Lewis acid–base catalyst were studied *via* FT-IR, FESEM, TGA, EDS-MAP, XRD, VSM, and BET. Some unique characteristics of the magnetic nanocatalysts enabled the development of the catalytic activity using a simple, efficient, green and eco-friendly protocol. The catalyst was reused several times without a loss of activity.

Introduction

Guar gum is a novel agrochemical processed from the endosperm of the cluster bean (*Cyamopsis tetragonoloba*). It is largely used in the form of guar gum powder as an additive in food, pharmaceuticals, paper, textiles, explosives, oil well drilling, and the cosmetics industry.[1,2] Industrial applications of guar gum are possible because of its ability to form hydrogen bonds with water molecules. Thus, it is chiefly used as a thickener and stabilizer.[3,4]

Increasing awareness of green chemistry and other biological processes has inspired the development of an eco-friendly approach for the synthesis of nanoparticles because of their advantages, such as facile synthesis, cost-effectiveness, and compatibility with biomedical applications as well as large-scale commercial production.[5] In recent years, many interesting methods have been applied for the green preparation of nano-sized magnetic particles.[6]

The modern focus on reducing pollution in organic reactions has led to the rise of heterogeneous catalytic systems as effective methods for waste reduction.[7,8] Catalysts are now being immobilized on various supports, with iron oxide magnetic nanoparticles (Fe_3O_4 MNPs) playing a crucial role owing to their low toxicity and superparamagnetism.[9,10] The combination of organic and inorganic materials at the nanoscale is increasingly used for its catalytic potential. Immobilizing catalysts on Fe_3O_4 MNPs enables easy separation without cumbersome methods such as centrifugation or filtration. These magnetic nanoparticles have been widely used in various organic transformations for their high activity levels.[11] The 4*H*-pyrimido[2,1-*b*]benzothiazole derivatives are compounds used in the preparation of drugs.[12,13] Recent studies have shown that these compounds can function as anti-tumor, anti-inflammatory, anti-bacterial and anti-fungal materials.[14–17] Therefore, owing to the significant biological and therapeutic relevance of 4*H*-pyrimido[2,1-*b*]benzothiazole, various synthetic strategies, including one-step and multi-step methods, have been reported.[18] One of the most attractive methods for the synthesis of 4*H*-pyrimido[2,1-*b*]benzothiazole is based on multi-component reactions (MCRs).[19] The synthesis of 4*H*-pyrimido[2,1-*b*]benzothiazole is a three-component condensation reaction between aldehyde, β-ketoester and 2-aminobenzothiazole.[20,21] Some of the catalysts that have previously been used for the synthesis of these products are Fe_3O_4@nano-cellulose-TiCl,[22] nano-kaolin/Ti^{4+}/Fe_3O_4,[23] nano-Fe_3O_4@SiO_2-$TiCl_3$,[24] Fe_3O_4@nano-cellulose/Cu(II),[25] FNAOSiPPEA/Cu(II),[26] and Fe_3O_4@nano-dextrin-OPO_3H_2.[27]

Despite the remarkable achievements for the synthesis of 4*H*-pyrimido[2,1-*b*]benzothiazole derivatives, there are limitations for some of these catalysts, such as inefficient separation of the catalyst from reaction mixtures, non-recyclability, and environmental limitations. Furthermore, this reaction was performed without a catalyst under harsh reaction conditions.[28]

Herein, we demonstrate a simple, environmentally friendly, and cost-effective method to prepare highly stable dispersions

[a]*Department of Organic Chemistry, Faculty of Chemistry, University of Kashan, Kashan, I. R. Iran. E-mail: bamoniri/kashanu.ac.ir*

[b]*Department of Chemistry, College of Science, Yazd University, Yazd, I. R. Iran. E-mail: fmirjalili/yazd.ac.ir*

of a magnetic nanoparticle catalyst. The catalyst is based on a Lewis acid derived from a natural biopolymer and is applied for the synthesis of pyrimido[2,1-*b*]benzothiazoles.

Results and discussion

We report the synthesis and characterization of nano guar gum/BF_3/Fe_3O_4 for the synthesis of 4*H*-pyrimido[2,1-*b*]benzothiazoles *via* the condensation reaction of ethyl acetoacetate, aromatic aldehydes, and 2-amino benzothiazole (Scheme 1).

The structure of nano guar gum/BF_3/Fe_3O_4 as a bio-based Lewis acid catalyst, was confirmed by Fourier transform infrared (FT-IR) spectroscopy, field emission scanning electron microscopy (FESEM), X-ray diffraction (XRD), thermogravimetric analysis (TGA), energy-dispersive X-ray spectroscopy (EDS-map), Brunauer–Emmett–Teller (BET) surface area measurement, and vibrating sample magnetometry (VSM).

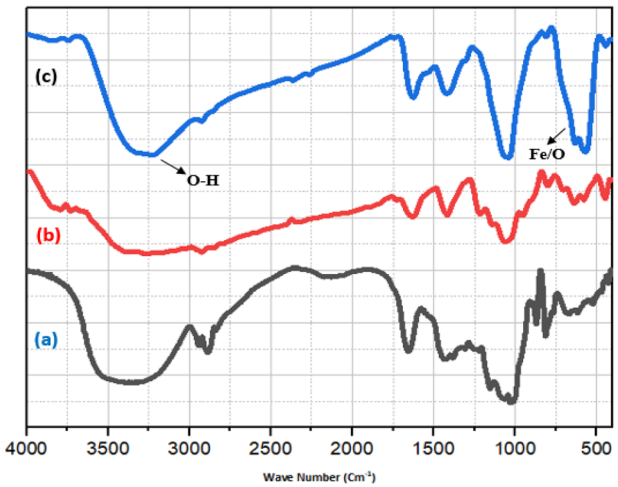

Fig. 1 FT-IR spectra of (a) guar gum, (b) nano guar gum/BF_3, and (c) nano guar gum/BF_3/Fe_3O_4.

FT-IR spectroscopy of nano guar gum/BF_3/Fe_3O_4

The FT-IR spectra of guar gum, nano guar gum/BF_3, and nano guar gum/BF_3/Fe_3O_4 are shown in Fig. 1. The FT-IR spectrum of guar gum (Fig. 1a) shows distinct peaks at 3389 cm^{-1}, 2942 cm^{-1}, and 1154 cm^{-1}, which are related to O–H, C–H, and C–O vibrational stretching, respectively. In the nano guar gum/BF_3/Fe_3O_4 spectrum (Fig. 1c), a distinct peak at 568 cm^{-1} is attributed to the Fe–O stretching vibration. In addition, the broad peak at 3400 cm^{-1} is attributed to the stretching vibration of O–H group.

FESEM and particle size distribution histogram of guar gum and nano guar gum/BF_3/Fe_3O_4

The particle size of guar gum (Fig. 2a) and nano guar gum/BF_3/Fe_3O_4 (Fig. 2b) was studied using field emission scanning

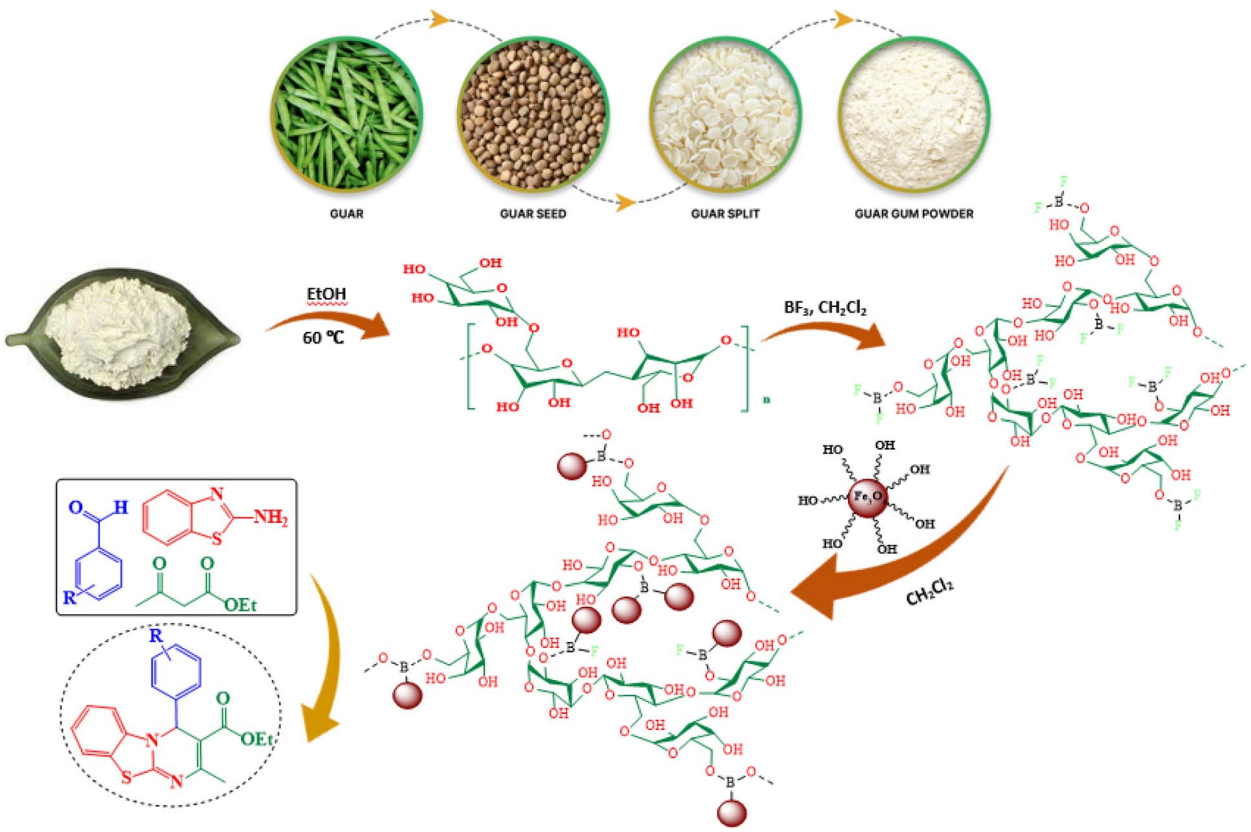

Scheme 1 Preparation of nano guar gum/BF_3/Fe_3O_4/for the synthesis of 4*H*-pyrimido[2,1-*b*]benzothiazoles.

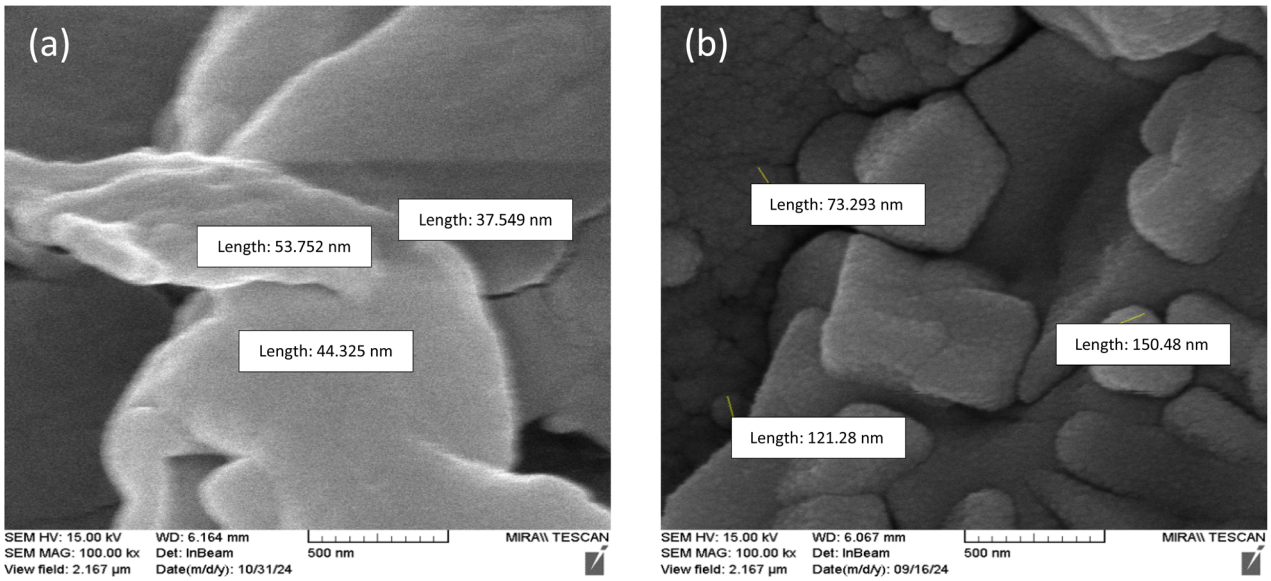

Fig. 2 FESEM images of (a) guar gum, and (b) nano guar gum/BF_3/Fe_3O_4.

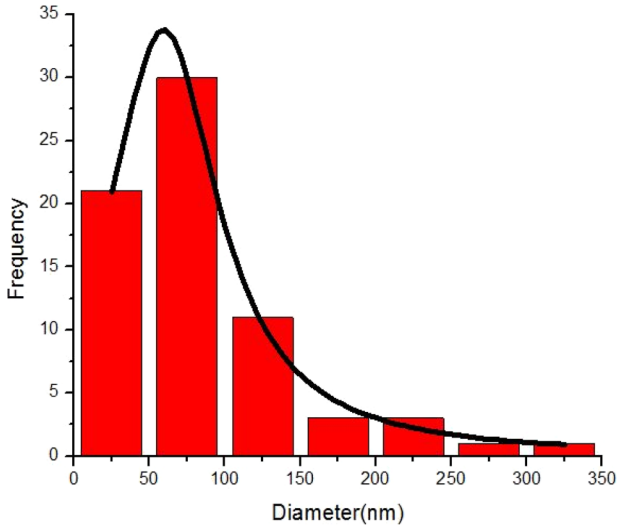

Fig. 3 Particle size distribution histogram nano guar gum/BF_3/Fe_3O_4.

electron microscopy (FESEM) and particle size distribution histogram and was found to be less than 100 nm (Fig. 2 and 3).

TGA of nano guar gum/BF_3/Fe_3O_4

Fig. 4 shows the TGA and DTA curves of guar gum, and nano guar gum/BF_3/Fe_3O_4.

The thermal gravimetric analysis pattern of guar gum was detected by heating from 50 °C to 450 °C (Fig. 4a). Weight loss (10%) occurred at temperatures between 50 and 100 °C, which is related to the removal of guar gum moisture. The main weight loss (55%) was observed in the range of 225–310 °C, due to the burning of guar gum. The next stage of weight loss (33.5%) occurred in the temperature range of 310–450 °C. The yield of guar gum char at 450 °C is 1.5% of the original weight. The nanocatalyst showed a small initial weight loss at a temperature lower than 100 °C due to the removal of absorbed water and other organic solvents. At temperatures higher than 100 °C (180–300 °C), the highest weight loss is observed in the TGA curve, which was probably due to the decomposition of guar gum and BF_3 from the catalyst.

XRD of nano guar gum/BF_3/Fe_3O_4

The XRD patterns of guar gum (Fig. 5a), Fe_3O_4 NPs (Fig. 5b), and nano guar gum/BF_3/Fe_3O_4 (Fig. 5c) are shown in Fig. 4. The signals in 2θ equal to 22° and 16° are related to the guar gum and, several peaks appeared at $2\theta = 31°$, 35°, 43°, 53°, 56°, and 61°, indicating that the original Fe_3O_4 crystalline structure was not destroyed.

VSM of nano guar gum/BF_3/Fe_3O_4

The magnetic properties of the Fe_3O_4 nanoparticles (Fig. 6a) and nano guar gum/BF_3/Fe_3O_4 (Fig. 6b) were measured using a vibrating sample magnetometer (VSM) at a temperature of 300 K. The obtained results are shown in the form of magnetization curves in Fig. 6. According to these curves, the value of the specific saturation magnetization (M_s) of the Fe_3O_4 nanoparticles is about 47 emu g^{-1}, which is reduced to 40 emu g^{-1} during the process of coating with guar gum and then connecting BF_3 on the surface of the guar gum. Despite the use of Lewis acid BF_3, the magnetism of the catalyst remains very high, and it can be easily separated from the reaction medium using an external magnet (Fig. 6). In addition, the samples exhibit zero coercivity and magnetic hysteresis, indicating their superparamagnetic behaviour at room temperature.

EDX and EDS-map of nano guar gum/BF_3/Fe_3O_4

The elemental composition of the nano guar gum/BF_3/Fe_3O_4 catalyst was determined by EDX. As shown in Fig. 7, the

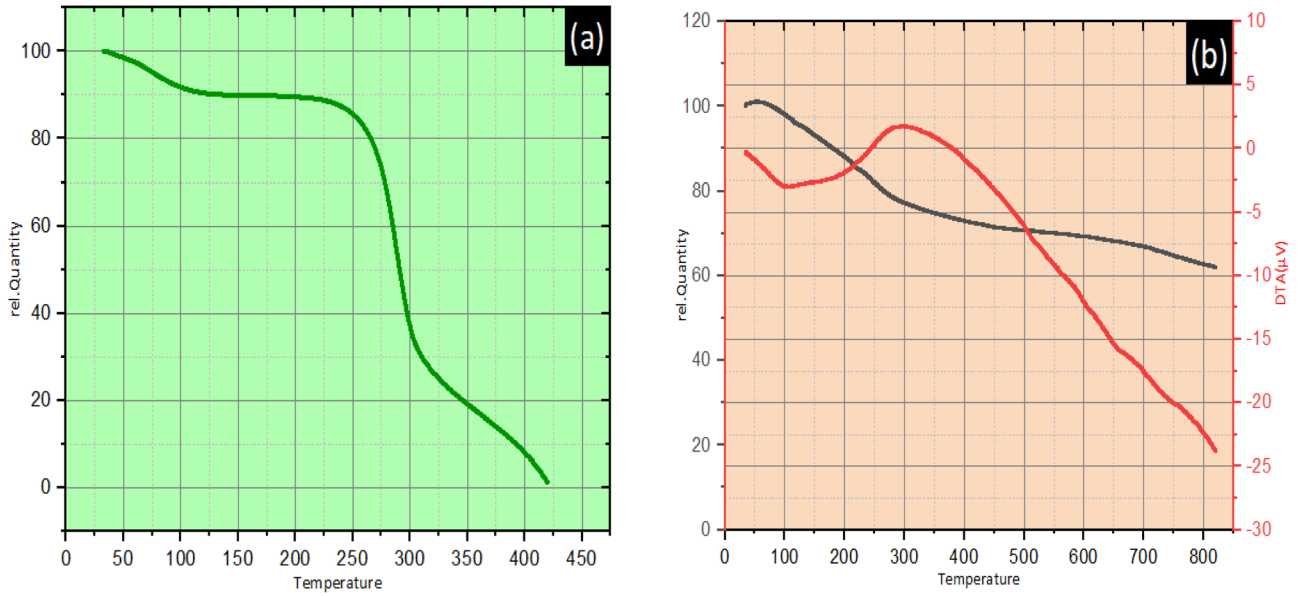

Fig. 4 TGA/DTA curves of (a) guar gum and (b) nano guar gum/BF_3/Fe_3O_4.

presence of Fe, O, C, B, and F signals prove the catalyst structure. The percentage composition of Fe, C, O, F, and B elements is 42.35, 26.4, 18.52, 9.52, and 3.21% respectively. According to the results of the EDS-mapping analysis in Fig. 8, these elements are homogeneously distributed on the surface of the nanocatalyst.

Inductively coupled plasma (ICP) spectroscopy was used to determine the iron content in the nano-guar gum/BF_3/Fe_3O_4 catalyst, which was 53% before and 44% after the reaction.

BET measurements of nano guar gum/BF_3/Fe_3O_4

The BET (Brunauer–Emmett–Teller) surface area of the prepared nanocatalyst was obtained by nitrogen adsorption and desorption measurements (Fig. 9). The N_2 isotherms related to the type IV isotherm in the IUPAC classification have shown H_3 type rings, which can indicate the existence of mesopores and also have non-hard pores. As shown in Table 1, according to BJH (Barrett–Joyner–Halenda) model analysis, the pore diameters were 30.466 m^2 g^{-1}, 0.1217 cm^3 g^{-1}, and 15.511 nm, respectively.

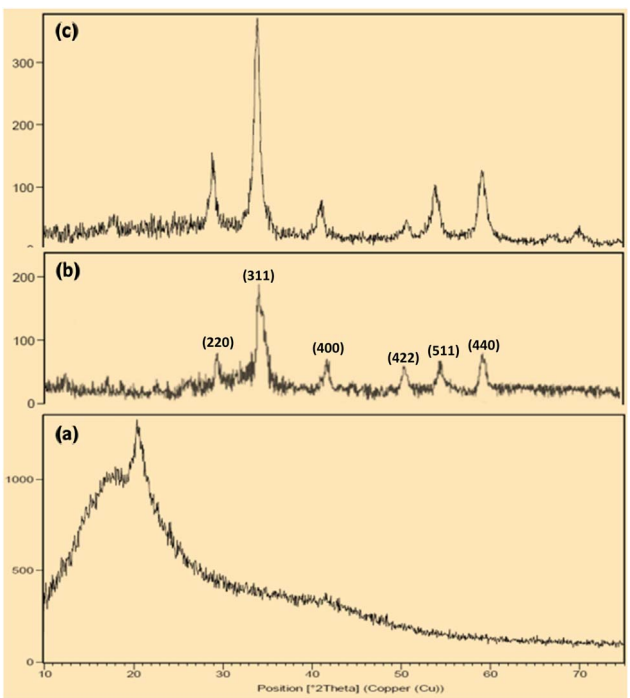

Fig. 5 XRD patterns of (a) guar gum (b) Fe_3O_4 NPs, and (c) Fe_3O_4/guar gum/BF_3.

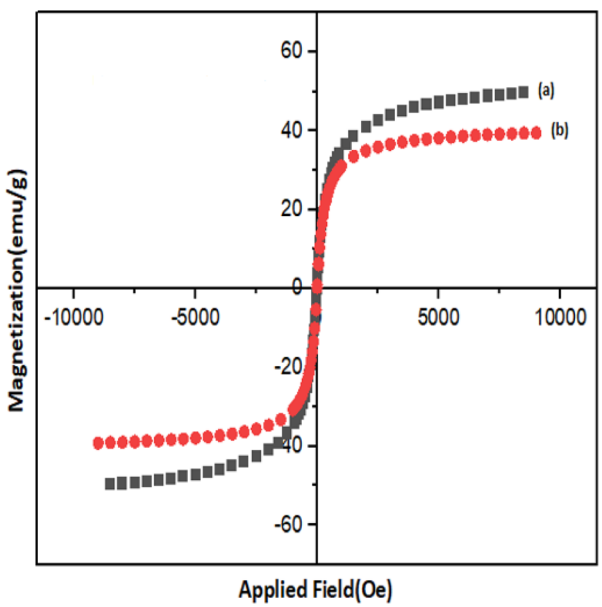

Fig. 6 VSM analysis of (a) Fe_3O_4 NPs, and (b) nano guar gum/BF_3/Fe_3O_4.

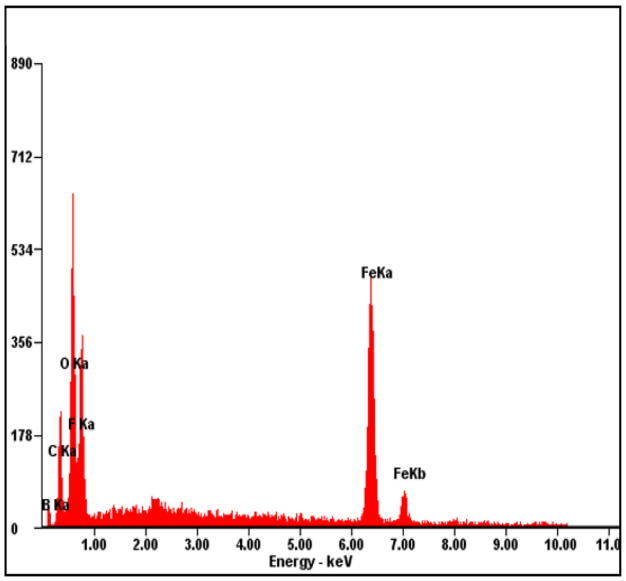

Fig. 7 EDS diagram of nano guar gum/BF_3/Fe_3O_4.

Catalyst activity of nano guar gum/BF_3/Fe_3O_4

The optimization study (Table 2) clearly demonstrates that the amount of catalyst, reaction temperature, and solvent play a crucial role in determining the yield and reaction time. Increasing the catalyst loading from 0.005 g to 0.02 g resulted in a significant increase in product yield and a remarkable reduction in reaction time, highlighting the importance of a higher number of accessible Lewis acidic sites in promoting the reaction. Likewise, increasing the temperature from 35 to 80 °C markedly enhanced the reaction efficiency, and under optimized conditions (0.02 g catalyst at 80 °C under solvent-free conditions), the highest yield of 96% was obtained within only 1.4 h. Examination of the solvent effects revealed that the use of ethanol or water provided inferior results compared to the solvent-free system. For instance, only a 42% yield was obtained in ethanol at room temperature, and even at elevated temperatures, the yield remained lower than that under solvent-free conditions. These findings emphasize that solvent-free conditions offer superior efficiency due to the increased effective collisions between reactant molecules and the absence of dilution of the catalytically active sites.

To evaluate the contribution of each component of the catalyst, control experiments were conducted using guar gum or BF_3 alone, which afforded only 57% and 51% yield, respectively. This comparison clearly indicates a synergistic effect among the three constituents, namely guar gum, BF_3, and Fe_3O_4. In this system, guar gum acts as a natural support and stabilizing matrix for the nanoparticles, BF_3 provides the necessary Lewis acid centers for carbonyl activation, and Fe_3O_4 increases the active surface area and enables facile magnetic separation of the catalyst. Altogether, the combination of these three components significantly enhanced the catalytic performance and led to increased yields in the target reaction.

The catalytic performance of nano guar gum/BF_3/Fe_3O_4 was further examined in the synthesis of 4*H*-pyrimido[2,1-*b*]benzothiazoles using various substituted aromatic aldehydes, and the results are summarized in Table 3.

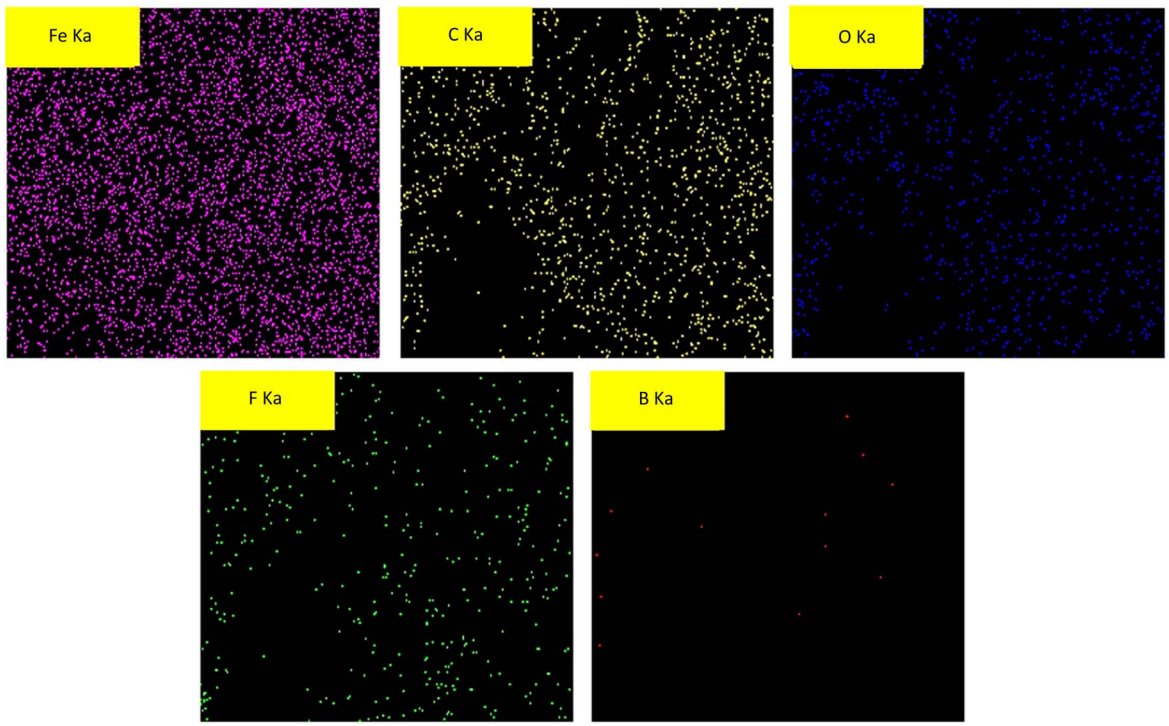

Fig. 8 Maps of nano guar gum/BF_3/Fe_3O_4.

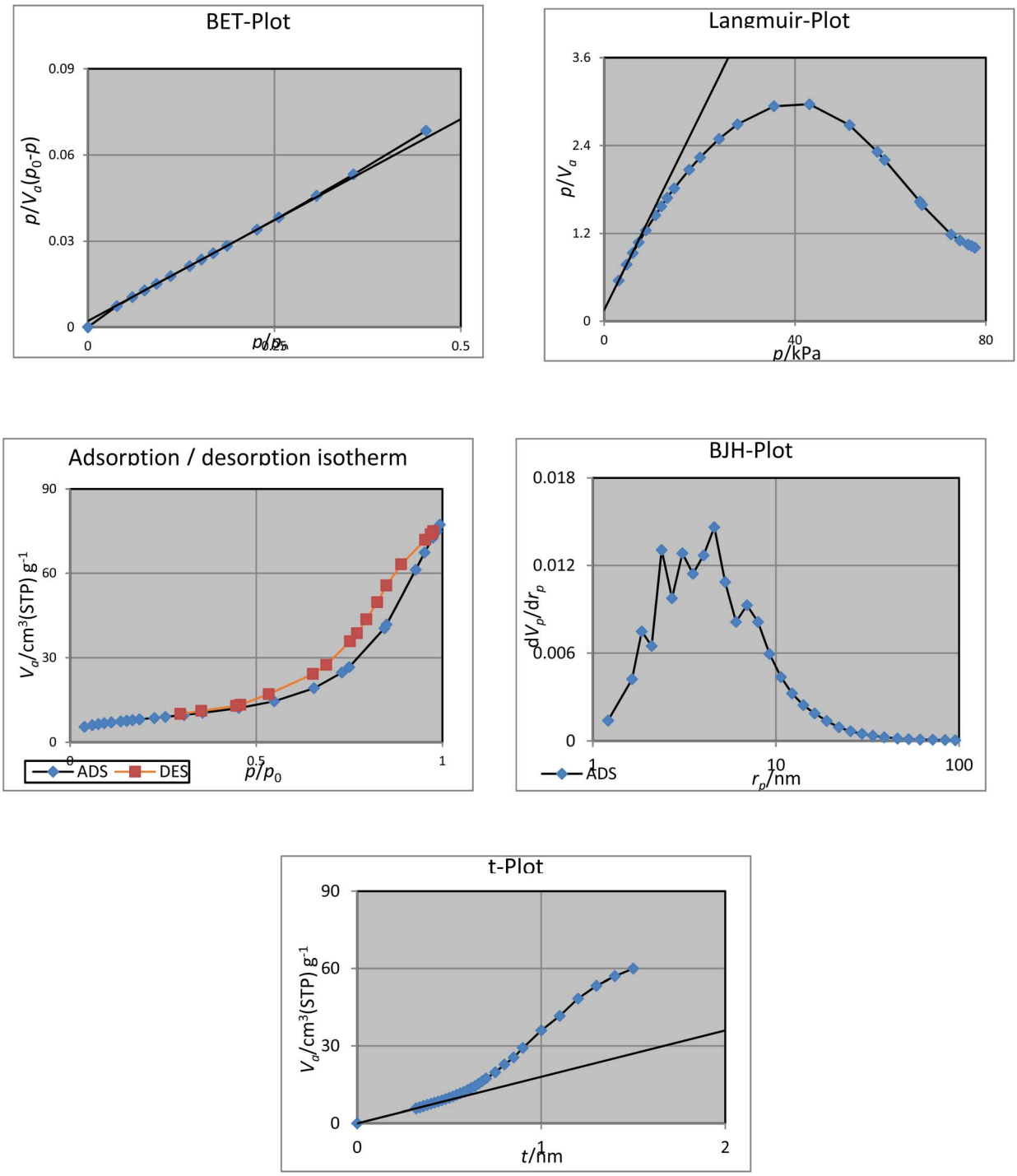

Fig. 9 N_2 adsorption (blue line)-desorption (red line) isotherm and corresponding diagrams showing the pore size distributions (BJH, BET, Langmuir, *t*-plot).

The electronic nature of the substituents on the aldehydes strongly influenced the reaction outcome. Aromatic aldehydes bearing electron-withdrawing groups, such as nitro substituents at the *ortho*, *meta*, or *para* positions, afforded higher yields in shorter times. Notably, 2-nitrobenzaldehyde delivered the product in 92% yield within only 60 min, which was attributed to the increased electrophilicity of the carbonyl carbon, facilitating the initial Knoevenagel condensation step. Conversely, aldehydes containing electron-donating groups, such as –OCH_3 or –OH, exhibited lower reactivity and produced lower yields (75% and 77%, respectively). This reduction in efficiency may be ascribed to the decreased electrophilicity of the carbonyl group as well as possible steric or hydrogen-

Table 1 Parameters obtained from the porosity analysis

BET plot		
V_m	6.9997	[cm^3 (STP) g^{-1}]
$a_{s,BET}$	30.466	[m^2 g^{-1}]
C	67.264	
Total pore volume ($p/p_0 = 0.990$)	0.1181	[cm^3 g^{-1}]
Mean pore diameter	15.511	[nm]
Langmuir plot		
V_m	7.5497	[cm^3 (STP) g^{-1}]
$a_{s,Lang}$	32.86	[m^2 g^{-1}]
B	0.875	
t plot		
Plot data	Adsorption branch	
a_1	27.755	[m^2 g^{-1}]
V_1	0	[cm^3 g^{-1}]
BJH plot		
Plot data	Adsorption branch	
V_p	0.1217	[cm^3 g^{-1}]
$r_{p,peak}$ (area)	4.61	[nm]
a_p	42.196	[m^2 g^{-1}]

bonding interactions that hinder the approach of 2-aminobenzothiazole to the aldehyde carbonyl.

In addition to electronic effects, steric factors also played an important role. Substrates with bulky or sterically hindered substituents, such as 2,4-dichlorobenzaldehyde and 2-hydroxynaphthaldehyde, required longer reaction times and produced relatively lower yields, indicating that steric hindrance restricts the access of the reactants to the activated carbonyl center. Overall, the data clearly demonstrate that the designed nanocatalyst accelerates the synthesis of 4*H*-pyrimido[2,1-*b*]benzothiazoles and maintains high efficiency across a broad range of substrates, with yields that are strongly correlated with the electronic and steric properties of the substituents.

To compare the efficiency of this magnetite bio-based nanocatalyst with other catalysts for the synthesis of 4*H*-pyrimido[2,1-*b*]benzothiazole derivatives, a summary of the results was collected in Table 4. The reaction efficiency of this catalyst is greater than that of other catalysts, and the reaction time is shorter than that of others.

Reusability of nano guar gum/BF_3/Fe_3O_4

To confirm the recyclability of the nano catalyst, after the completion of the reaction, the catalyst can be separated from

Table 2 Optimization of reaction conditions for the synthesis of 4*H*-pyrimido[2,1-*b*]benzothiazoles[a]

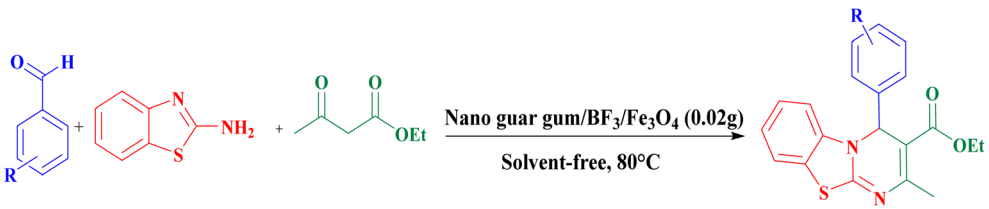

Entry	Conditions: Solvent, temp. (°C), catalyst (g)	Time (h)	Yield[b] (%)
1	—, r.t., nano guar gum/BF_3/Fe_3O_4 (0.005)	5	53
2	—, r.t., nano guar gum/BF_3/Fe_3O_4 (0.01)	5	68
3	—, r.t., nano guar gum/BF_3/Fe_3O_4 (0.015)	5.30	68
4	—, r.t., nano guar gum/BF_3/Fe_3O_4 (0.02)	3.30	86
5	—, 35, nano guar gum/BF_3/Fe_3O_4 (0.02)	3.30	85
6	—, 55, nano guar gum/BF_3/Fe_3O_4 (0.02)	3	87
7	—, 65, nano guar gum/BF_3/Fe_3O_4 (0.02)	2.30	87
8	—, 80, nano guar gum/BF_3/Fe_3O_4 (0.005)	3	86
9	—, 80, nano guar gum/BF_3/Fe_3O_4 (0.01)	2.30	87
10	**—, 80, nano guar gum/BF_3/Fe_3O_4(0.02)**	**1.40**	**96**
11	—, 80, nano guar gum/BF_3/Fe_3O_4 (0.03)	2	88
12	—, 80, —	4.30	51
13	EtOH, r.t., nano guar gum/BF_3/Fe_3O_4 (0.02)	4	79
14	EtOH, 80, nano guar gum/BF_3/Fe_3O_4 (0.02)	3.30	83
15	H_2O, 80, nano guar gum/BF_3/Fe_3O_4 (0.02)	5	41
16	—, 80, nano guar gum/BF_3 (0.02)	2.30	80
17	—, 80, nano guar gum (0.02)	4.5	57
18	—, 80, BF_3 (0.02)	1.5	70
19	—, 80, Fe_3O_4 (0.02)	3.50	36

[a] Conditions: benzaldehyde (1 mmol), ethyl acetoacetate (1 mmol), and 2-amino benzothiazole (1 mmol), solvent free. [b] Isolated yield.

Table 3 Nano guar gum/BF_3/Fe_3O_4 catalyzed the synthesis of 4*H*-pyrimido[2,1-*b*]benzothiazoles[a]

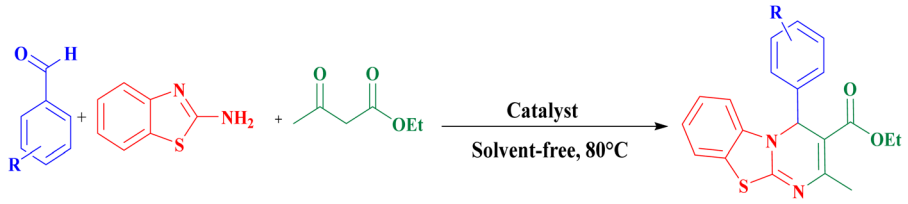

		Nano guar gum		Nano guar gum/BF_3		Nano guar gum/BF_3/Fe_3O_4		
Entry	R	Time (min)	Yield[b] (%)	Time (min)	Yield[b] (%)	Time (min)	Yield[b] (%)	mp. (ref.)
1	H	270	57	150	80	100	96	177–180 (ref. 22)
2	4-Cl	195	80	80	85	65	90	89–91 (ref. 29)
3	2,4-$(Cl)_2$	240	71	75	83	70	89	132–134 (ref. 30)
4	4-Br	120	84	100	90	65	95	112–115 (ref. 31)
5	2-NO_2	135	69	60	79	55	85	121–123 (ref. 32)
6	3-NO_2	120	86	60	81	45	93	223–225 (ref. 33)
7	4-NO_2	100	86	60	78	60	96	172–174 (ref. 34)
8	3-OH	260	58	120	75	90	86	260–262 (ref. 27)
9	4-OH	200	61	120	80	100	88	209–212 (ref. 24)
10	2-OEt	230	66	105	71	90	85	173–176 (ref. 25)
11	2,4-$(OMe)_2$	250	75	90	78	75	87	165–167 (ref. 32)
12	2-Hydroxynaphthalen	180	68	120	83	105	89	220–222

[a] Conditions: aldehyde (1 mmol), ethyl acetoacetate (1 mmol), 2-amino benzothiazole (1 mmol), 80 °C, Solvent free, catalyst (0.02 g). [b] Isolated yield.

Table 4 Comparison of nano-Fe_3O_4/BF_3/guar gum with other catalysts for the synthesis of 4*H*-pyrimido[2,1-*b*]benzothiazoles

	Conditions			
Entry	Catalyst, solvent, temp. (°C)	Time (h)	Yield (%)	Ref.
1	Nano-kaolin/Ti^{4+}/Fe_3O_4, —, 100 °C	1.50	95	23
2	Nano-Fe_3O_4@SiO_2-$TiCl_3$, —, 100 °C	0.50	90	24
3	FNAOSiPPEA/Cu(II) (0.04 g), —, 100 °C	1	97	26
4	Fe_3O_4@NCs/Sb(v) (0.03), —, 90 °C	0.50	98	34
5	Nano guar gum/BF_3/Fe_3O_4 (0.02), —, 80 °C	1.40	96	This work

the reaction mixture with a magnet, and after washing with chloroform ($CHCl_3$) and drying at ambient temperature, it can be reused for the synthesis of 4*H*-pyrimido[2,1-*b*] benzothiazoles. Therefore, the reusability of the catalyst for the model reaction was evaluated for the synthesis of 4*H*-pyrimido [2,1-*b*]benzothiazoles (Fig. 10).

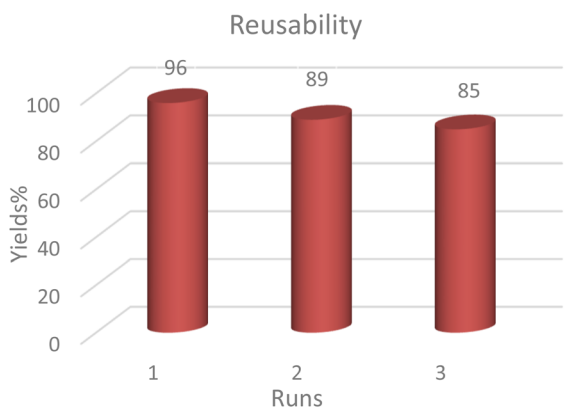

Fig. 10 Reusability of nano guar gum/BF_3/Fe_3O_4 for the synthesis of 4*H*-pyrimido[2,1-*b*]benzothiazoles.

Proposed mechanism for synthesis of 4*H*-pyrimido[2,1-*b*] benzothiazoles

The synthesis of 4*H*-pyrimido[2,1-*b*]benzothiazoles proceeds *via* a multicomponent reaction involving aromatic aldehydes, ethyl acetoacetate, and 2-aminobenzothiazole in the presence of a boron-based catalyst. Initially, a Knoevenagel condensation between the aldehyde and ethyl acetoacetate affords an α,β-unsaturated intermediate, facilitated by activation of the carbonyl group through hydrogen bonding interactions with the boron catalyst. This activated olefin undergoes a Michael-type addition with the nucleophilic amino group of 2-amino-benzothiazole, followed by intramolecular cyclization and proton transfer. Subsequent dehydration results in the formation of the fused heterocyclic 4*H*-pyrimido[2,1-*b*]benzothiazole framework. The boron-based catalyst plays a key role in

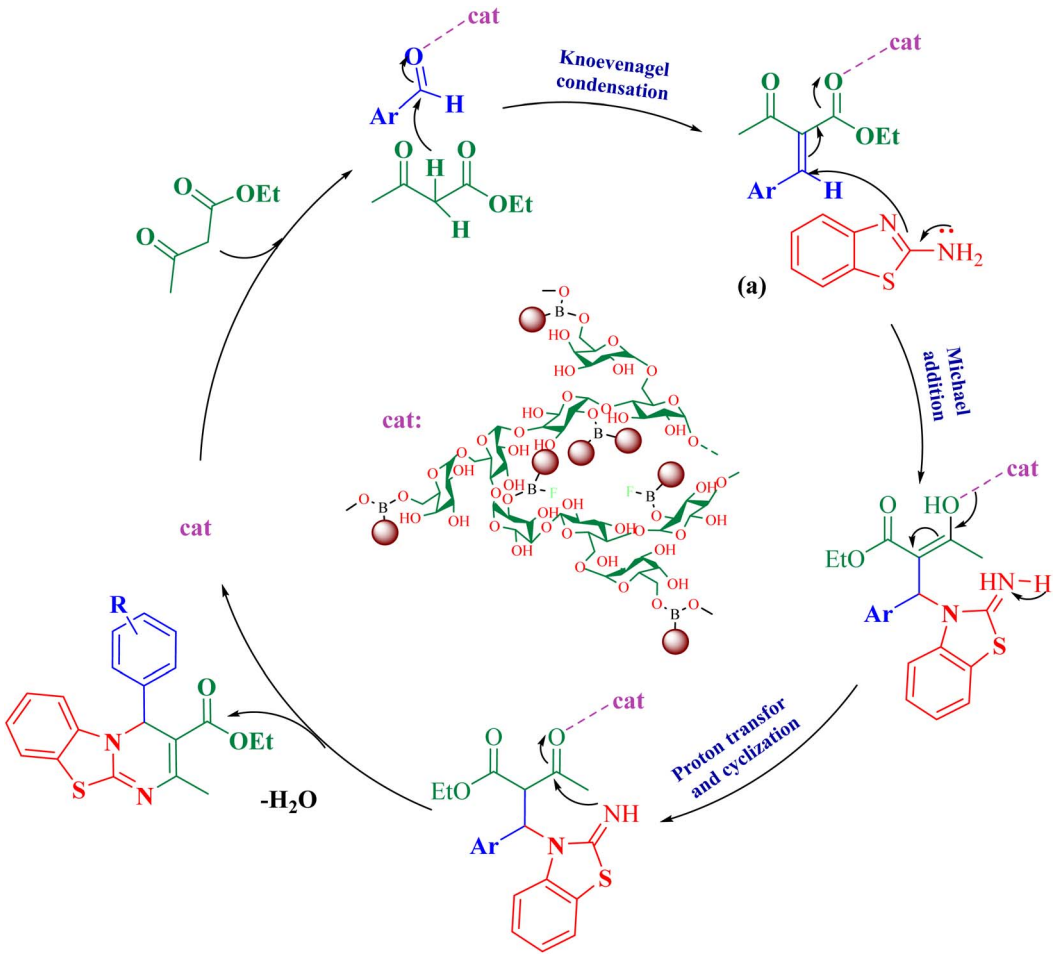

Scheme 2 Proposed mechanism for synthesis of 4*H*-pyrimido[2,1-*b*]benzothiazoles.

promoting enolate formation, stabilizing transition states, and enhancing the rate and selectivity of the reaction (Scheme 2).

Experimental section

Materials and methods

Chemicals were purchased from Merck, Fluka, and Aldrich Chemical Companies. ^{1}H NMR and ^{13}C NMR spectra were recorded at 400 and 100 MHz, respectively. Fourier transform infrared (FT-IR) spectroscopy measurements (in KBr pellets or ATR) were recorded on a Bruker spectrometer. Melting points were determined on a Büchi B-540 apparatus. The X-ray diffraction (XRD) pattern was obtained by a Philips Xpert MPD diffractometer equipped with a Cu Kα anode ($k = 1.54$ Å) in the 2θ range from 10 to 80°.

A Mira 3-XMU was used for the field emission scanning electron microscopy (FESEM). Vibrating sample magnetometry (VSM) measurements were obtained using a vibrating sample magnetometer (Meghnatis Daghigh Kavir Co. Kashan Kavir, Iran). Energy-dispersive X-ray spectroscopy (EDS) of the nanocatalyst was measured by an EDS instrument and Phenom pro X. The EDX-MAP micrographs were obtained on the MIRA II detector SAMX (France). Thermal gravimetric analysis (TGA) was conducted using the "STA 504" instrument. A BELSORP MINI II nitrogen adsorption apparatus (Japan) was used for recording Brunauer–Emmett–Teller (BET) surface area measurements of the nanocatalyst at 77 K.

Purification of the nano guar gum

White guar gum powder is prepared in different processes.[35] According to the results of FESEM, the size of guar gum particles is less than 50 nm. Therefore, to remove possible contamination and impurities, 5 g of nano guar gum was treated with 20 mL of EtOH at 60 °C for 4 h under reflux conditions. To remove possible impurities present in the purchased guar gum, it was washed several times with ethanol before use. Subsequently, the nano guar gum was filtered and washed with distilled water, and the yield was 99%.

Preparation of Fe_3O_4

In a 250 mL flask, 100 mL of 0.05 M acetic acid (CH_3COOH) was added. After that, $FeCl_3 \cdot 6H_2O$ (3.51 g, 13 mmol) and $FeCl_2 \cdot 4H_2O$ (1.29 g, 6.5 mmol) were added and the solution was stirred for 6 h at 80 °C. Then, 8 mL of NH_4OH (25%), was added dropwise, and the solution was stirred for 45 min. The

precipitated brown products were isolated from the solution by a magnet, washed 3 times with distilled water, and dried in an oven at 80 °C for 4 h. Fe_3O_4 was prepared using the co-precipitation method.

Synthesis of nano guar gum/BF_3/Fe_3O_4

In a 100 mL flask, 1 g of nano guar gum/BF_3 catalyst is added to the Fe_3O_4 (0.3 g) solution in 20 mL of dichloromethane, which is dispersed by ultrasonic waves, and the final mixture is vigorously stirred by a mechanical stirrer for 6 h at 60 °C. Then the prepared catalyst nano guar gum/BF_3/Fe_3O_4 is separated from the reaction mixture by an external magnet, washed with dichloromethane, and dried.

General synthesis of 4*H*-pyrimido[2,1-*b*]benzothiazoles

For the synthesis of 4*H*-pyrimido[2,1-*b*]benzothiazoles, in a 50 mL round-bottom flask, 2-aminobenzothiazole (1 mmol), aldehyde (1 mmol), ethyl acetoacetate (1 mmol), and nano-Fe_3O_4/guar gum/BF_3 (0.02 g) were mixed under solvent-free conditions. The reaction mixture was stirred at 80 °C for the durations specified in Table 2. After the end of the reaction (TLC), ethyl acetate : *n*-hexane 6 : 3 the mixture was dissolved in hot ethanol (5 mL), and the catalyst was separated by an external magnet. Then, by the dropwise addition of water (1 mL) to the reaction mixture, the precipitates of the product appeared as a pure solid in high yield.

Conclusion

A magnetite guar gum-based nanocatalyst was prepared, characterized, and used for the synthesis of 4*H*-pyrimido[2,1-*b*]benzothiazoles. The prepared nano guar gum/BF_3/Fe_3O_4 shows high catalytic activity and good reusability. This method is non-toxic and biodegradable, and it may be used to prepare other biopolymer-based nanocatalysts for more interesting reactions.

Conflicts of interest

There are no conflicts to declare.

Data availability

All data generated or analyzed during this study are included in this published article and its supplementary information (SI). Supplementary information is available. See DOI: **https://doi.org/10.1039/d5na00201j**.

Acknowledgements

The Research Council of University of Kashan and Yazd University is gratefully acknowledged for the financial support for this work.

References

1 J. Anandan and S. Sivasankar, *Ultrason. Sonochem.*, 2018, **40**, 1–10.
2 S. Pandey and S. B. Mishra, *Carbohydr. Polym.*, 2014, **113**, 525.
3 T. Baran, N. Y. Baran and A. Mentes, *Int. J. Biol. Macromol.*, 2019, **132**, 1147–1154.
4 E. Abdel-Halim, M. El-Rafie and S. S. Al-Deyab, *Carbohydr. Polym.*, 2011, **85**, 692–697.
5 M.-N. Chen, L.-P. Mo, Z.-S. Cui and Z.-H. Zhang, *Curr. Opin. Green Sustainable Chem.*, 2019, **15**, 27–37.
6 S. B. Singh and P. K. Tandon, *J. Energy Chem. Eng.*, 2014, **2**, 106–115.
7 J. Safari and L. Javadian, *Iran. J. Catal.*, 2016, **6**, 58–64.
8 F. Kiani, D. Elhamifar and S. Kargar, *Nanoscale Adv.*, 2025, **7**, 1552–1560.
9 S. M. R. Mousavi and K. Rad-Moghadam, *Nanoscale Adv.*, 2025, **7**, 1901–1913.
10 A. O. Moghanlou, M. Pourshahi, S. Atabak and N. M. Tarighi, *Iran. J. Catal.*, 2023, **13**, 187–192.
11 F. Dadvar and D. Elhamifar, *Nanoscale Adv.*, 2024, **6**, 5398.
12 Y. Yu, W.-F. Lu, Z.-J. Yang, N. Wang and X.-Q. Yu, *Bioorg. Chem.*, 2021, **107**, 104534.
13 Y. Yu, W. Zhang, Q.-T. Gong, Y.-H. Liu, Z.-J. Yang, W.-X. He, N. Wang and X.-Q. Yu, *J. Biotechnol.*, 2020, **324**, 91–98.
14 A. B. Atar, Y. S. Jeong and Y. T. Jeong, *Tetrahedron*, 2014, **70**, 5207–5213.
15 P. K. Sharma, A. Amin and M. Kumar, *Open Med. Chem. J.*, 2020, **1**, 14.
16 M. N. Bhoi, M. A. Borad, D. J. Jethava, P. T. Acharya, E. A. Pithawala, C. N. Patel, H. A. Pandya and H. D. Patel, *Eur. J. Med. Chem.*, 2019, **177**, 12–31.
17 M. R. Anizadeh, M. A. Zolfigol, M. Yarie, M. Torabi and S. Azizian, *Res. Chem. Intermed.*, 2020, **46**, 3945–3960.
18 B. Laha, A. R. Tiwari, E. Gravel, E. Doris and I. N. Namboothiri, *Org. Biomol. Chem.*, 2024, **22**, 1346.
19 R. Talaei and A. Olyaei, *Iran. J. Catal.*, 2016, **6**, 339–343.
20 M. N. Bhoi, M. A. Borad, A. P. Solanki and H. D. Patel, *Phosphorus, Sulfur Silicon Relat. Elem.*, 2023, **198**, 822–835.
21 P. K. Sahu, P. K. Sahu, Y. Sharma and D. D. Agarwal, *J. Heterocycl. Chem.*, 2014, **51**, 1193–1198.
22 S. Azad and B. B. F. Mirjalili, *RSC Adv.*, 2016, **6**, 96928–96934.
23 B. B. F. Mirjalili and R. Soltani, *RSC Adv.*, 2019, **9**, 18720–18727.
24 S. A. Fazeli-Attar and B. B. F. Mirjalili, *Res. Chem. Intermed.*, 2018, **44**, 6419–6430.
25 N. Safajoo, B. B. F. Mirjalili and A. Bamoniri, *RSC Adv.*, 2019, **9**, 1278–1283.
26 D. Mallah and B. B. F. Mirjalili, *BMC Chem.*, 2022, **16**, 45.
27 A. Dehghani Tafti, B. B. F. Mirjalili, N. Salehi and A. Bamoniri, *J. Iran. Chem. Soc.*, 2022, **19**, 4377–4388.
28 Z. Moghadasi, A. N. Fajer, A. M. Abudken and H. A. Al-Bahrani, *Nanomater. Chem.*, 2023, **1**(1), 24–31.
29 S. S. Gong, R. Kong, C. Zheng, C. Fan, C. Wang, D. Z. Yang, Z. Z. Chen, S. Duo, S. Pu and Q. Sun, *J. Mater. Chem.*, 2021, **9**, 10029–10036.

30 K. Khazenipour, F. Moeinpour and F. S. Mohseni-Shahri, *J. Chin. Chem. Soc.*, 2021, **68**, 121–130.
31 A. R. Moosavi-Zare, H. Goudarziafshar and P. Fashi, *Res. Chem. Intermed.*, 2020, **46**, 5567.
32 B. B. F. Mirjalili and F. Aref, *Res. Chem. Intermed.*, 2018, **44**, 4519–4531.
33 S. Singh and J. Lal, *SN. Appl. Sci.*, 2020, **2**, 1–9.
34 S. S. Hosseinikhah and B. B. F. Mirjalili, *Polycyclic Aromat. Compd.*, 2022, **42**, 1013–1022.
35 G. Sharma, S. Sharma, A. Kumar, H. Ala'a, M. Naushad, A. A. Ghfar, G. T. Mola and F. J. Stadler, *Carbohydr. Polym.*, 2018, **199**, 534–545.